HHS Public Access

Author manuscript

Nat Cell Biol. Author manuscript; available in PMC 2013 March 01.

Published in final edited form as:

Nat Cell Biol. 2012 September ; 14(9): 950–957. doi:10.1038/ncb2560.

The BBSome controls IFT assembly and turnaround in cilia

Qing Wei[1,*], **Yuxia Zhang**[1,*], **Yujie Li**[1], **Qing Zhang**[1], **Kun Ling**[2,3], and **Jinghua Hu**[1,2,3,†]

[1]Division of Nephrology and Hypertension, Mayo Clinic, Rochester, Minnesota, USA

[2]Mayo Translational PKD Center, Mayo Clinic, Rochester, Minnesota, USA

[3]Department of Biochemistry and Molecular Biology, Mayo Clinic, Rochester, Minnesota, USA

Abstract

The bidirectional movement of intraflagellar transport (IFT) particles, which are composed of motors, IFT-A and IFT-B subcomplexes, and cargos, is required for cilia biogenesis and signaling [1, 2]. A successful IFT cycle depends on the massive IFT particle to be properly assembled at the ciliary base and turned around from anterograde to retrograde transport at the ciliary tip. However, how IFT assembly and turnaround are regulated *in vivo* remains elusive. From a whole-genome mutagenesis screen in *C. elegans*, we identified two hypomorphic mutations in *dyf-2* and *bbs-1* as the only mutants showing normal anterograde IFT transport but defective IFT turnaround at the ciliary tip. Further analyses revealed that the BBSome [3, 4], a group of conserved proteins affected in human Bardet-Biedl syndrome (BBS) [5], assembles IFT complexes at the ciliary base, then binds to anterograde IFT particle in a DYF-2- (an ortholog of human WDR19) and BBS-1-dependent manner, and lastly reaches the ciliary tip to regulate proper IFT recycling. Our results unravel the BBSome as the key player regulating IFT assembly and turnaround in cilia.

Phylogenetically conserved IFT machinery mediates the bidirectional movement of IFT cargos that are required for the biogenesis, maintenance, and signaling of cilia [1]. At cilia tip, IFT particles need to be remodeled to enable the motor exchange, cargo release/loading, and turnaround [6]. In *Chlamydomonas*, IFT-A and IFT-B dissociate after being transported to the flagella tip and then IFT-B reassociates with IFT-A prior to retrograde IFT [7]. To dissect the molecular pathway controlling IFT turnaround at cilia tip, we initiated a genome-wide ethyl methanesulfonate (EMS) mutagenesis screen in *C. elegans* to search for mutants with abnormal ciliary accumulation of the GFP-tagged IFT-B component OSM-6 (the ortholog of human IFT52). We reasoned that defective IFT turnaround should lead to IFT-B accumulation at the ciliary tip and compromise cilia formation. In *C. elegans*, mutants with

---

†Correspondence and requests for materials should be addressed to hu.jinghua@mayo.edu, Tel: (507) 293-3497; Fax: (507) 266-9315.
*These authors contributed equally to this work

Contributions:

J.H. conceived the initial concept for the screen. J.H., Q.W., Y.L., and Y.Z. performed the screening and mapped the mutants. Q.W. and Y.Z. generated transgenic animals and performed image analysis with the support of Q.Z. Y.Z. carried out all microinjections. Q.W. and K.L. carried out biochemical assays with the support of Y.Z. K.L. and J.H. wrote the manuscript with the contribution of Q.W., Y.Z., Y.L., and Q.Z.

abnormal cilia formation cannot take up fluorescent dye and are thus called dye-filling defective (Dyf) [8]. We screened ~60,000 haploid genomes and retrieved 608 Dyf mutants. Out of these, 158 Dyf mutants showed strong OSM-6::GFP accumulation in cilia. However, 154 out of 158 mutants showed severely truncated cilia and no IFT transport, either anterograde or retrograde, which suggest mutations in essential IFT structural genes. In contrast, four recessive mutants, *jhu555, jhu590, jhu598,* and *jhu616,* exhibited frequent IFT movements and normal (or only slightly truncated) cilia, indicative of defective IFT recycling at the ciliary tip.

Mapping of *jhu616* identified a glycine-to-arginine (G361R) substitution at the highly conserved WD40 domain of DYF-2 protein (Fig. 1a, b), a known IFT component that is the ortholog of human WDR19 (also known as IFT144 in *Chlamydomonas*) [9]. Introducing a wild-type *dyf-2* gene fully rescued *jhu616* (Fig. S1a & b). GFP-tagged DYF-2^{G361R} mutant protein cannot efficiently enter the cilia and tends to accumulate around the ciliary base (Fig. S1c). Interestingly, *dyf-2(jhu616)* mutants differ from the reported *dyf-2(m160) null* mutants. The former possess almost normal cilia in length as well as active IFT movements, while the latter show severely truncated cilia and completely disrupted IFT transport [9] (Fig. 1d, e), indicating that G361R mutation is a hypomorphic allele that does not affect the major role of DYF-2 as an IFT structural protein. Remarkably, kymograph analyses revealed that, in *dyf-2(jhu616),* IFT-B component OSM-6 showed characteristic anterograde IFT movement, but lost almost all retrograde IFT movements (Fig. 1e). The severely impaired retrograde IFT explains the accumulation of OSM-6::GFP at the ciliary tip and suggests a key function for DYF-2 WD40 domain in regulating IFT-B recycling at the ciliary tip.

In *C. elegans*, two kinesin motors, the canonical heterotrimeric kinesin-II and homodimeric OSM-3 (the ortholog of human KIF17), coordinate anterograde IFT transport [10, 11]. The amphid and phasmid cilia in *C. elegans* contain two segments, middle doublet and distal singlet segments (Fig. 1c). Kinesin-II and OSM-3 cooperate in moving the same IFT particle along the middle doublet at 0.7μm/s, and then OSM-3 kinesin alone moves the IFT particle along the distal singlet at the faster rate of 1.3μm/s. If IFT-A and IFT-B dissociate, IFT-A will be transported by kinesin-II at 0.5μm/s and IFT-B will be transported by OSM-3 at 1.3μm/s in middle segments [10, 11]. In *dyf-2(jhu616),* we found that the IFT velocity of OSM-6::GFP in middle segments is comparable to wild-type rate (Table S1), indicating that the integrity of anterograde IFT particles is normal. To further determine whether IFT-A and IFT-B associate in *dyf-2(jhu616),* we performed bimolecular fluorescence complementation (BiFC) assay. BiFC assay was developed for direct visualization of protein-protein interaction in the same macromolecular complex in their natural environment of living cells [12]. As shown in Fig. S2a, IFT-A component CHE-11 and IFT-B component IFT-20 showed fluorescence complementation in either wild-type or *dyf-2(jhu616*), indicative of the association between IFT-A and IFT-B subcomplexes. In drastic contrast, no fluorescence complementation was observed in *dyf-2(m160)* null mutant, which is also consistent with the previous finding that IFT integrity is totally disrupted in *dyf-2(m160)* null worms [9].

Similar to OSM-6, in *dyf-2*(*jhu616),* all other IFT-B components examined also showed active anterograde movements, but lost most of the retrograde IFT movements and accumulate at the ciliary tip (Fig. 2a–c, e, f).

In *Chlamydomonas*, IFT144 (the homolog of DYF-2) is an IFT-A component [13]. A temperature-sensitive mutation in *ift144* gene (*fla15*) results in the accumulation of IFT-B and retrograde IFT motor dynein in the bulges of normal-length flagella as well as reduced retrograde IFT velocities and frequencies [14–16]. *fla15* mutants resemble other IFT-A mutants in *Chlamydomonas* [14, 15]. Similarly, in *ift144*^{twt} mice that carry a partial loss-of-function IFT144 protein, cilia still form normally but accumulate IFT-B at cilia tip and lack detectable IFT-A proteins inside cilia [17]. Since dynein and IFT-A components are the key players of the retrograde IFT machinery [15, 18–20], the accumulation of IFT-B in *fla15 flagella* or *ift144*^{twt} cilia is likely due to the defective retrograde IFT machinery. To examine if the accumulation of IFT-B in *dyf-2(jhu616)* is also due to the defective retrograde transport, we examined the IFT-A marker CHE-11 (the ortholog of human IFT140), the retrograde IFT motor dynein light chain XBX-1 (the ortholog of human D2LIC) and the IFT-A associated kinesin-II motor KAP-1. Remarkably, we found that dynein as well as other IFT-A markers localize properly to cilia and show no accumulation at cilia tip, and most importantly, all these markers exhibited normal bidirectional IFT transport (Fig. 2d, g, h). The comparable anterograde IFT rates between IFT-A and IFT-B components confirm again that IFT-A and IFT-B do associate together in anterograde transports (Table S1). Taken together, these findings indicate that, not like *fla15 Chlamydomonas* or *ift144*^{twt} mice, the retrograde IFT machinery in *dyf-2(jhu616)* is still functional, and the ciliary accumulation of IFT-B in *dyf-2(jhu616)* is because IFT-B components fail to be assembled into the functional IFT-A-dynein machinery prior to retrograde IFT transports. Thus, our observations reveal a role for the WD40 domain of DYF-2 as the key factor in reassembling IFT-B subcomplex into IFT-A-dynein retrograde machinery.

To further understand why only IFT reassembly at the ciliary tip is specifically affected in *dyf-2(jhu616)*, we examined other proteins that were reported to associate with the IFT complex. The BBSome proteins are a group of eight conserved proteins whose etiologies are associated with cilia dysfunction and the autosomal recessive ciliopathy Bardet-Biedl syndrome [3–5, 21]. Controversy has been surrounding the role of the BBSome in the context of cilia. Knocking down of BBS5 in *Chlamydomonas* leads to the absence of flagella [22]. However, *bbs4 Chlamydomonas* mutants show normal flagella but defective IFT transport [23]. *bbs* knockdown zebrafish show delayed dynein-dependent intracellular retrograde transport of melanosome and defective ciliogenesis in ciliated organ Kupffer's vesicle [24, 25]. Knockout mouse models of various *bbs* genes fail to form sperm flagella, but form primary cilia in other organs examined [26–28]. However, the observations that *bbs* knockout mice exhibit mislocalization of rhodopsin in photoreceptor, misshaped kidney cilia, and abnormal bulges inside ependymal and airway cilia also suggest a role for the BBSome in IFT transport [28–30]. In *bbs-7* and *bbs-8* null worms, IFT-A and IFT-B dissociate in anterograde IFT transport, resulting in IFT-A moving alone with kinesin-II and IFT-B moving alone with OSM-3 [10, 31]. It's thus suggested that the BBSome hold IFT-A and IFT-B together during IFT transport to offset the mechanical competing force generated between the faster motor OSM-3 and the slower motor kinesin-II [32].

Surprisingly, in *dyf-2(jhu616)* animals, we found that all BBS proteins examined strongly accumulated around the ciliary base. Some of them (BBS-1, BBS-4) totally lost the ciliary

localization; the others (BBS-2, -5, -7, -8, -9) only showed very dim ciliary staining when compared to wild-type animals (Fig. 3). Most importantly, all BBS proteins completely lost IFT movement, indicating the complete dissociation between the BBSome and the moving IFT particles (Fig. 3). To determine whether worm BBS proteins really form a complex, we performed BiFC analyses. In wild-type animals, fluorescence complementation can be observed in BBS-1–BBS-7 and BBS-1–BBS-9 pair, indicative of the coexistence of these three BBS proteins in the same complex (Fig. S3a). This finding is also consistent with the prediction that mammalian BBS1, 7, and 9 locate closely to each other in the BBSome [3]. The fluorescence complementation between BBS proteins was totally disrupted in *bbs* null mutants examined (Fig. S3b), which further suggest worm BBS proteins form a macromolecular complex in their native environment. Strikingly, in *dyf-2(jhu616)* mutants, the BBSome still formed, but was only restricted to cilia base (Fig. S3b–c).

In *dyf-2(jhu616)* animals, the fact that IFT-A and IFT-B still associate in anterograde IFT in the absence of the entire BBSome demonstrates that the BBSome does not act as an indispensable component for the IFT machinery to stabilize the binding of IFT-A–IFT-B during IFT transport. The conclusion is also supported by the observation made in *Chlamydomonas* that the BBSome is substoichiometric to the IFT particle during IFT transport and, thus, not an integral part of IFT machinery [23]. Combined with the observation that IFT-A and IFT-B dissociate in *bbs* null mutants, we proposed that the *in vivo* function for the BBSome is to regulate the assembly of the IFT particles at the ciliary base. After IFT particles are assembled at the ciliary base, the BBSome binds to the IFT particle like a cargo but not a structural component. We further hypothesized that the BBSome may play a similar role in IFT reassembly and turnaround at cilia tip. In *dyf-2(jhu616)*, although the BBSome lost the association with anterograde IFT particles, it is still functional at the ciliary base and results in normal IFT assembly and anterograde transport; while the absence of the BBSome at cilia tip leads to defective IFT reassembly and the accumulation of IFT-B components at cilia tip (Fig. 5).

The key evidence supporting the mechanical competition model for the BBSome is that if either one of the two kinesin motors is absent in *bbs* null mutants, IFT-A and IFT-B will reassociate again in anterograde IFT transport [32]. We then examined *bbs-7; osm-3* double mutants. OSM-3 is the anterograde motor for IFT-B. We found that, in ~50% of *bbs-7; osm-3* animals, IFT-B components show no anterograde IFT movement at all; in the rest half of them, only a few IFT-B-containing particles can be observed in anterograde transport (Fig. S4a). Furthermore, in a given time period, equivalent numbers of IFT-B-containing and IFT-A–containing particles can be observed in wild type, *bbs-7*, or *osm-3* single mutant, whereas the average number of IFT-B–containing particles (~4 particles /min) is only about one tenth of that of IFT-A–containing ones (~40 particles /min) in *bbs-7; osm-3* animals (Fig. S4c). In all *bbs-7; osm-3* animals examined, IFT-B proteins show few retrograde IFT and still accumulate at the ciliary tip (Fig. S4a, S4b). Taken together, these results demonstrate that, in *bbs-7; osm-3* double mutants, most IFT-B cannot associate with IFT-A even in the absence of the mechanical competing force. These observations indicate that the major role for the BBSome in cilia is to efficiently assemble IFT particles at both cilia base and tip.

To further verify our model, we mapped the other three Dyf mutants. *jhu555*, *jhu590*, and *jhu598* were mapped to *bbs-9*, *bbs-7*, and *bbs-1*, respectively. Kymograph analyses indicated that IFT-A and IFT-B separate and move at different rates in anterograde IFT in *bbs-7(jhu590)* (encodes BBS-7 with a nonsense mutation at Q546 site) and *bbs-9(jhu555)* (encodes BBS-9 with a nonsense mutation at Q171 site) mutants just like in other reported *bbs null* mutants (Table S1). IFT-B components tend to accumulate in various *bbs* mutants, as revealed in published papers [10, 31, 33]. However, the underlying mechanism of the accumulation of IFT-B in *bbs null* animals differs from that in *dyf-2(jhu616)*. IFT-A, the essential player for retrograde IFT, cannot be transported into cilia distal segments to reach cilia tip in *bbs null* mutants [10]. Absence of IFT-A at cilia tip would naturally lead to the IFT-B accumulation in *bbs null* mutants due to the defective retrograde IFT transport. Whereas in *dyf-2(jhu616)* animals, IFT-A can reach cilia tip and perform retrograde IFT, but IFT-B fails to reassociate with IFT-A prior to retrograde IFT, which leads to the accumulation of IFT-B at cilia tip.

Remarkably, the defects of *bbs-1(jhu598)* animals completely phenocopy the observations in *dyf-2(jhu616)*: IFT-A and IFT-B associate in anterograde but not retrograde IFT and IFT-B accumulates at the ciliary tip (Fig. 4b, c, Table S1). BiFC assay also confirmed that IFT-A can still associate with IFT-B in *bbs-1(jhu598)* (Fig. S2b). Sequencing results indicated that *bbs-1(jhu598)* encodes a BBS-1 mutant with a glycine-to-aspartic acid change at the highly conserved G207 site (G207D) (Fig. 4a). Compared to the strong ciliary targeting of wild-type BBS-1 protein, GFP-tagged BBS-1^{G207D} only accumulated around the ciliary base (Fig. S5a). Overexpression of BBS-1^{G207D} caused a mild dominant-negative effect in dye-filling assay (Fig. S5b). Like in *dyf-2(jhu616)* animals, all BBSome proteins strongly accumulate around the ciliary base and show no IFT movement in *bbs-1(jhu598)* (Fig. 4d, Fig. S5c–g). We then built *dyf-2(jhu616); bbs-1(jhu598)* double mutant. In *dyf-2(jhu616); bbs-1(jhu598)*, IFT-A proteins still show wild-type ciliary localization, whereas IFT-B accumulation is more severe and extends to most part of the cilium, and as expected, BBS proteins strongly accumulate around ciliary base and show no IFT movement (Fig. S5h–i).

We next assessed DYF-2 ciliary localization in *bbs-1(jhu598)* animals. Compared to the wild-type worms, the ciliary targeting of DYF-2 was significantly reduced in *bbs-1(jhu598)* mutants; whereas the remaining ciliary DYF-2 still showed normal IFT movement in both directions (Fig. 4e–f). These data reminded us of the behavior of DYF-2^{G361R} protein (Fig. S1). It appears that the dissociation between the BBSome and the IFT particle may also affect the efficient incorporation of DYF-2 into anterograde IFT particles. To test this possibility, we determined whether DYF-2 and BBS-1 interact with each other. Results from BiFC analyses suggest that DYF-2 locates near BBS-1, BBS-7 and BBS-9 in the native IFT particles; however the G361R mutation in DYF-2 protein abolished the fluorescence complementation, indicating the dissociation between DYF-2^{G361R} and the BBSome (Fig. 4g). Results from biochemical analyses using mammalian cells further support the association of DYF-2 and BBS-1. As shown in Figure 4h, when coexpressed, mouse WDR19 (the homolog of DYF-2) and BBS1 (the homolog of BBS-1) show strong interaction. However, a mutation at G341 in WDR19 (WDR19^{G341R}, mimicking the worm DYF-2^{G361R} mutant) significantly reduces this association. And the binding between

WDR19^{G341R} and BBS1^{G222D} (mimicking the worm BBS-1^{G207D}) was almost totally abolished. These findings indicate that the two conserved sites in DYF-2 and BBS-1 identified in our study probably mediate the interaction between the BBSome and the IFT machinery.

Taken together, we conclude that the BBSome is required for assembling IFT particles at both ciliary base and tip. In *dyf-2(jhu616)* or *bbs-1(jhu598)* cilia, the BBSome is still functional at the ciliary base supported by the observation that IFT-A and IFT-B associate in anterograde transport, but the docking of the BBSome onto moving IFT particles is disrupted. The absence of the BBSome at the cilia tip leads to the defective recycling of IFT complex (Fig. 5).

The IFT machinery assembles at the ciliary base to load the cargos, including membrane receptors, structural proteins, and signaling molecules; transports them to the ciliary tip; and then unloads the cargos, which are used to build cilia and maintain sensory function [1, 6]. On the other hand, retrograde transport not only functions to recycle IFT machinery to the ciliary base, but also is indispensable for ciliary signal transduction, such as sonic hedgehog signaling [34–36]. Interestingly, various ciliary roles have been proposed for the BBSome such as IFT integrity maintenance [10, 31, 33], cilia membrane biogenesis [3], cilia membrane protein targeting [37, 38], cilia signaling protein export [23], proteasomal function [39], and pericentriolar cargo trafficking [40]. The BBSome also shares the common structural features with COPI, COPII, and clathrin coats, and can directly recognize IFT cargos [38]. Combined with our findings that the BBSome controls IFT assembly at both ciliary base and tip, it is highly likely that the BBSome functions as a scaffold to organize IFT-A, IFT-B, ciliary membrane receptors, ciliary signaling molecules, and/or other IFT cargos into an entire unit and prepare it for IFT transport. Thus, the absence of the BBSome on IFT particles could compromise the loading of membrane receptors at the ciliary base and the IFT-mediated export of signaling molecules at the ciliary tip. Our data also suggest the WD40 domain of DYF-2 protein is critical for the association between the BBSome and IFT particles. Remarkably, in *ift144* mutant mice, several membrane proteins failed to enter primary cilia, indicative of the functional correlation between IFT144 and the BBSome [17]. Taken together, our findings not only provide mechanistic insights into the missing links in the ciliogenesis pathway, but also significantly advance our understanding of the pathophysiologies of cilia-related diseases.

Supplementary Material

Refer to Web version on PubMed Central for supplementary material.

Acknowledgments

We thank the *Caenorhabditis* Genetics Center, the Japanese Bioresource Project, Drs. Jonathan Scholey, Michele Leroux, and Maureen Barr for strains; and Dr. Andrew Fire for GFP vectors. J.H. and coworkers were supported by the National Institutes of Health research grant 1R01DK090038 and P30 center grant P30DK90728, a Pilot and Feasibility Award from the Mayo Clinic Center for Cell Signaling in Gastroenterology (P30DK084567), and the PKD Foundation Young Investigator Award 04YI09a. J. H. was also supported by FULK Career Development Award, Zell PKD Research Award, and Upjohn PKD Research Fund. K.L. was supported by National Cancer Institute (NCI; 1R01CA149039-01A1), Susan G. Komen for the Cure (KG100902), and National Institute of Diabetes and Digestive and Kidney Diseases (P30DK90728).

References

1. Pedersen LB, Rosenbaum JL. Intraflagellar transport (IFT) role in ciliary assembly, resorption and signalling. Current topics in developmental biology. 2008; 85:23–61. [PubMed: 19147001]
2. Scholey JM, Anderson KV. Intraflagellar transport and cilium-based signaling. Cell. 2006; 125:439–442. [PubMed: 16678091]
3. Nachury MV, et al. A core complex of BBS proteins cooperates with the GTPase Rab8 to promote ciliary membrane biogenesis. Cell. 2007; 129:1201–1213. [PubMed: 17574030]
4. Loktev AV, et al. A BBSome subunit links ciliogenesis, microtubule stability, and acetylation. Developmental cell. 2008; 15:854–865. [PubMed: 19081074]
5. Zaghloul NA, Katsanis N. Mechanistic insights into Bardet-Biedl syndrome, a model ciliopathy. The Journal of clinical investigation. 2009; 119:428–437. [PubMed: 19252258]
6. Rosenbaum JL, Witman GB. Intraflagellar transport. Nature reviews. 2002; 3:813–825.
7. Pedersen LB, Geimer S, Rosenbaum JL. Dissecting the molecular mechanisms of intraflagellar transport in chlamydomonas. Curr Biol. 2006; 16:450–459. [PubMed: 16527740]
8. Hedgecock EM, Culotti JG, Thomson JN, Perkins LA. Axonal guidance mutants of Caenorhabditis elegans identified by filling sensory neurons with fluorescein dyes. Developmental biology. 1985; 111:158–170. [PubMed: 3928418]
9. Efimenko E, et al. Caenorhabditis elegans DYF-2, an orthologue of human WDR19, is a component of the intraflagellar transport machinery in sensory cilia. Molecular biology of the cell. 2006; 17:4801–4811. [PubMed: 16957054]
10. Ou G, Blacque OE, Snow JJ, Leroux MR, Scholey JM. Functional coordination of intraflagellar transport motors. Nature. 2005; 436:583–587. [PubMed: 16049494]
11. Snow JJ, et al. Two anterograde intraflagellar transport motors cooperate to build sensory cilia on C. elegans neurons. Nature cell biology. 2004; 6:1109–1113. [PubMed: 15489852]
12. Hu CD, Chinenov Y, Kerppola TK. Visualization of interactions among bZIP and Rel family proteins in living cells using bimolecular fluorescence complementation. Molecular cell. 2002; 9:789–798. [PubMed: 11983170]
13. Cole DG, et al. Chlamydomonas kinesin-II-dependent intraflagellar transport (IFT): IFT particles contain proteins required for ciliary assembly in Caenorhabditis elegans sensory neurons. The Journal of cell biology. 1998; 141:993–1008. [PubMed: 9585417]
14. Iomini C, Li L, Esparza JM, Dutcher SK. Retrograde intraflagellar transport mutants identify complex A proteins with multiple genetic interactions in Chlamydomonas reinhardtii. Genetics. 2009; 183:885–896. [PubMed: 19720863]
15. Piperno G, et al. Distinct mutants of retrograde intraflagellar transport (IFT) share similar morphological and molecular defects. The Journal of cell biology. 1998; 143:1591–1601. [PubMed: 9852153]
16. Iomini C, Babaev-Khaimov V, Sassaroli M, Piperno G. Protein particles in Chlamydomonas flagella undergo a transport cycle consisting of four phases. The Journal of cell biology. 2001; 153:13–24. [PubMed: 11285270]
17. Liem KF Jr, et al. The IFT-A complex regulates Shh signaling through cilia structure and membrane protein trafficking. The Journal of cell biology. 2012; 197:789–800. [PubMed: 22689656]
18. Pazour GJ, Wilkerson CG, Witman GB. A dynein light chain is essential for the retrograde particle movement of intraflagellar transport (IFT). The Journal of cell biology. 1998; 141:979–992. [PubMed: 9585416]
19. Signor D, et al. Role of a class DHC1b dynein in retrograde transport of IFT motors and IFT raft particles along cilia, but not dendrites, in chemosensory neurons of living Caenorhabditis elegans. The Journal of cell biology. 1999; 147:519–530. [PubMed: 10545497]
20. Schafer JC, Haycraft CJ, Thomas JH, Yoder BK, Swoboda P. XBX-1 encodes a dynein light intermediate chain required for retrograde intraflagellar transport and cilia assembly in Caenorhabditis elegans. Molecular biology of the cell. 2003; 14:2057–2070. [PubMed: 12802075]

21. Fliegauf M, Benzing T, Omran H. When cilia go bad: cilia defects and ciliopathies. Nature reviews. 2007; 8:880–893.
22. Li JB, et al. Comparative genomics identifies a flagellar and basal body proteome that includes the BBS5 human disease gene. Cell. 2004; 117:541–552. [PubMed: 15137946]
23. Lechtreck KF, et al. The Chlamydomonas reinhardtii BBSome is an IFT cargo required for export of specific signaling proteins from flagella. The Journal of cell biology. 2009; 187:1117–1132. [PubMed: 20038682]
24. Tayeh MK, et al. Genetic interaction between Bardet-Biedl syndrome genes and implications for limb patterning. Human molecular genetics. 2008; 17:1956–1967. [PubMed: 18381349]
25. Yen HJ, et al. Bardet-Biedl syndrome genes are important in retrograde intracellular trafficking and Kupffer's vesicle cilia function. Human molecular genetics. 2006; 15:667–677. [PubMed: 16399798]
26. Fath MA, et al. Mkks-null mice have a phenotype resembling Bardet-Biedl syndrome. Human molecular genetics. 2005; 14:1109–1118. [PubMed: 15772095]
27. Mykytyn K, et al. Bardet-Biedl syndrome type 4 (BBS4)-null mice implicate Bbs4 in flagella formation but not global cilia assembly. Proceedings of the National Academy of Sciences of the United States of America. 2004; 101:8664–8669. [PubMed: 15173597]
28. Nishimura DY, et al. Bbs2-null mice have neurosensory deficits, a defect in social dominance, and retinopathy associated with mislocalization of rhodopsin. Proceedings of the National Academy of Sciences of the United States of America. 2004; 101:16588–16593. [PubMed: 15539463]
29. Shah AS, et al. Loss of Bardet-Biedl syndrome proteins alters the morphology and function of motile cilia in airway epithelia. Proceedings of the National Academy of Sciences of the United States of America. 2008; 105:3380–3385. [PubMed: 18299575]
30. Davis RE, et al. A knockin mouse model of the Bardet-Biedl syndrome 1 M390R mutation has cilia defects, ventriculomegaly, retinopathy, and obesity. Proceedings of the National Academy of Sciences of the United States of America. 2007; 104:19422–19427. [PubMed: 18032602]
31. Ou G, et al. Sensory ciliogenesis in Caenorhabditis elegans: assignment of IFT components into distinct modules based on transport and phenotypic profiles. Molecular biology of the cell. 2007; 18:1554–1569. [PubMed: 17314406]
32. Pan X, et al. Mechanism of transport of IFT particles in C. elegans cilia by the concerted action of kinesin-II and OSM-3 motors. The Journal of cell biology. 2006; 174:1035–1045. [PubMed: 17000880]
33. Blacque OE, et al. Loss of C. elegans BBS-7 and BBS-8 protein function results in cilia defects and compromised intraflagellar transport. Genes & development. 2004; 18:1630–1642. [PubMed: 15231740]
34. Tran PV, et al. THM1 negatively modulates mouse sonic hedgehog signal transduction and affects retrograde intraflagellar transport in cilia. Nature genetics. 2008; 40:403–410. [PubMed: 18327258]
35. May SR, et al. Loss of the retrograde motor for IFT disrupts localization of Smo to cilia and prevents the expression of both activator and repressor functions of Gli. Developmental biology. 2005; 287:378–389. [PubMed: 16229832]
36. Huangfu D, Anderson KV. Cilia and Hedgehog responsiveness in the mouse. Proceedings of the National Academy of Sciences of the United States of America. 2005; 102:11325–11330. [PubMed: 16061793]
37. Berbari NF, Lewis JS, Bishop GA, Askwith CC, Mykytyn K. Bardet-Biedl syndrome proteins are required for the localization of G protein-coupled receptors to primary cilia. Proceedings of the National Academy of Sciences of the United States of America. 2008; 105:4242–4246. [PubMed: 18334641]
38. Jin H, et al. The conserved Bardet-Biedl syndrome proteins assemble a coat that traffics membrane proteins to cilia. Cell. 2010; 141:1208–1219. [PubMed: 20603001]
39. Gerdes JM, et al. Disruption of the basal body compromises proteasomal function and perturbs intracellular Wnt response. Nature genetics. 2007; 39:1350–1360. [PubMed: 17906624]

40. Kim JC, et al. The Bardet-Biedl protein BBS4 targets cargo to the pericentriolar region and is required for microtubule anchoring and cell cycle progression. Nature genetics. 2004; 36:462–470. [PubMed: 15107855]

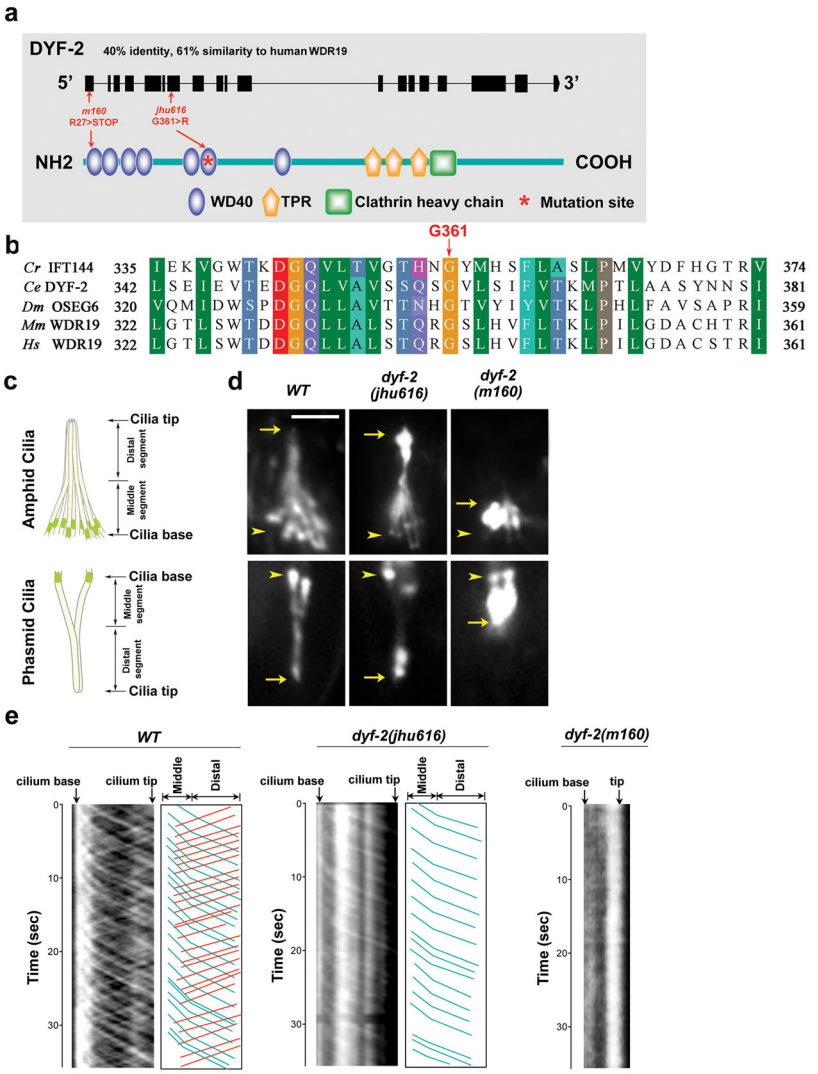

Figure 1. G361R mutation in the conserved WD40 domain of DYF-2 protein abolishes retrograde IFT transport of OSM-6

a, Schematic of DYF-2 protein and mutation sites. *m160* null allele possesses a nonsense mutation at the first exon. **b,** DYF-2 G361 is highly conserved across species. *Cr, Chlamydomonas reinhardtii; Ce, Caenorhabditis elegans; Dm, Drosophila melanogaster; Mm, Mus musculus; Hs, Homo sapiens.* **c,** In *C. elegans*, amphids in the head and phasmids in the tail are the primary ciliated sensory organs. Amphid and phasmid ciliary axonemes consist of a doublet 'middle segment' and a singlet 'distal segment.' Amphid channel cilia consist of 10 cilia, and phasmid channel cilia consist of 2 cilia. **d,** Fluorescence micrographs of cilia labeled with OSM-6::GFP. Compared to the severely truncated cilia in *dyf-2(m160)* animals, cilia in *dyf-2(jhu616)* are almost normal. OSM-6::GFP strongly accumulates at the ciliary tip in *dyf-2(jhu616).* Arrows and arrowheads indicate the tips and bases of cilia, respectively. Bar**,** 5 μm. **e,** Kymograph analyses of OSM-6::GFP movement in wild-type, *dyf-2(jhu616), and dyf-2(m160)* cilia. Kymographs (left panels) and corresponding cartoons (right panels) show visible OSM-6 anterograde (blue lines) and retrograde (red lines) IFT motilities. Compared to wild-type controls, the retrograde transport of OSM-6::GFP is

severely abrogated in *dyf-2(jhu616)* cilia, whereas no IFT movement can be detected in *dyf-2(m160) null* mutants.

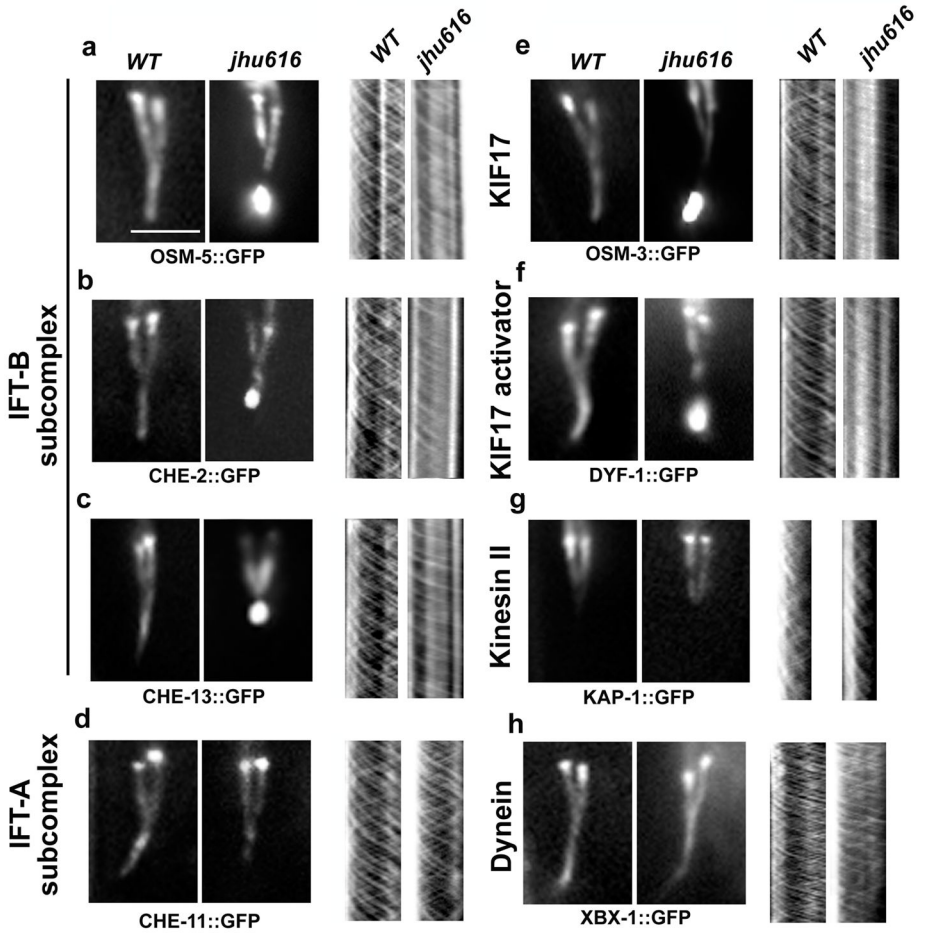

Figure 2. *dyf-2(jhu616)* animals show compromised IFT turnaround at the ciliary tip

Fluorescence micrographs of cilia labeled with various IFT markers (**a–h, left panels**) and corresponding kymographs (**a–h, right panels**). In *dyf-2(jhu616)*, IFT-B components OSM-5 (the ortholog of human IFT88) (**a**), CHE-2 (the ortholog of human IFT80) (**b**), and CHE-13 (the ortholog of human IFT57) (**c**), the IFT-B–associated kinesin motor OSM-3/KIF17 (**e**), and the OSM-3 activator DYF-1(the homolog of human TTC30B) (**f**) show consistent ciliary tip accumulation similar to OSM-6 (Fig. 1d) and exhibit severely abrogated retrograde IFT movement (**a–c, e–f, right panels**). In contrast, IFT-A components CHE-11 (the ortholog of human IFT140) (**d**) and the IFT-A–associated kinesin-II subunit KAP-1 (**g**) show no ciliary accumulation and exhibit both anterograde and retrograde IFT motilities at characteristic wild-type rates (Table S1). Note that kinesin-II only mediates IFT motility in the middle segments (**g**). As expected, the dynein light chain XBX-1 that is responsible for retrograde IFT movement shows no ciliary accumulation and moves normally in both directions (**h**). Bar**,** 5 μm.

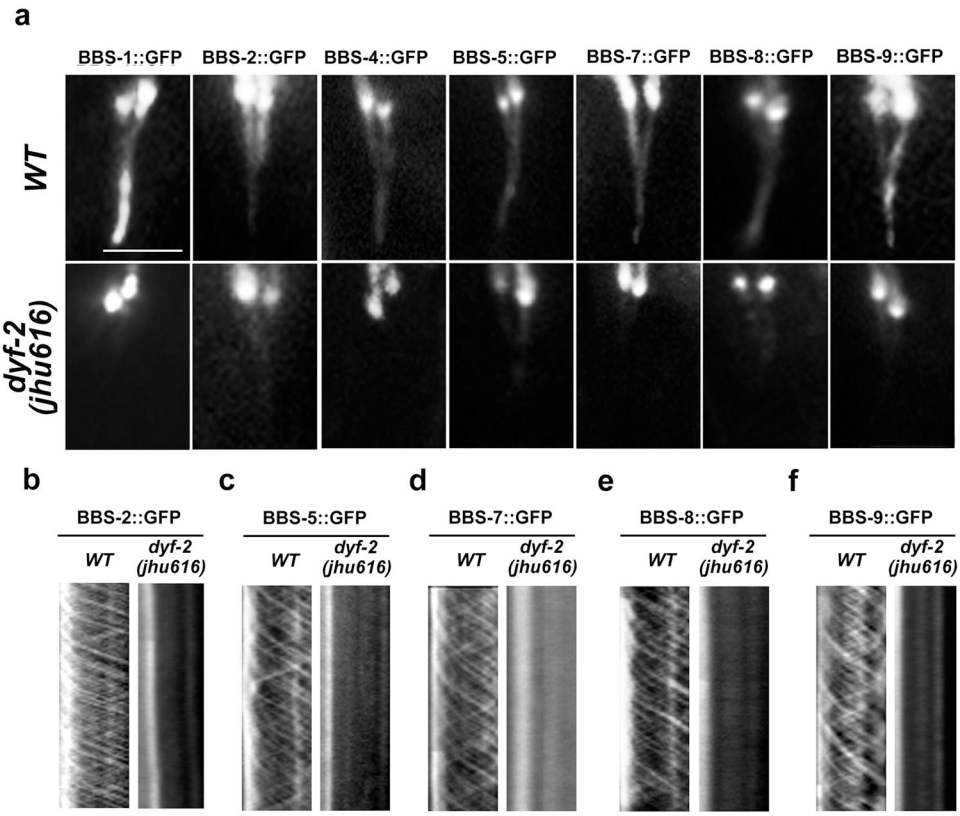

Figure 3. Lack of functional BBSome in *dyf-2(jhu616)* cilia

a, BBS proteins show either absent (BBS-1, BBS-4) or dramatically reduced (BBS-2, -5, -7, -8, and -9) ciliary localization in *dyf-2(jhu616)* animals. **b–f,** No IFT movements are detected for residual ciliary BBS-2, BBS-5, BBS-7, BBS-8, or BBS-9 in *dyf-2(jhu616)* cilia. In all panels: bar**,** 5 μm.

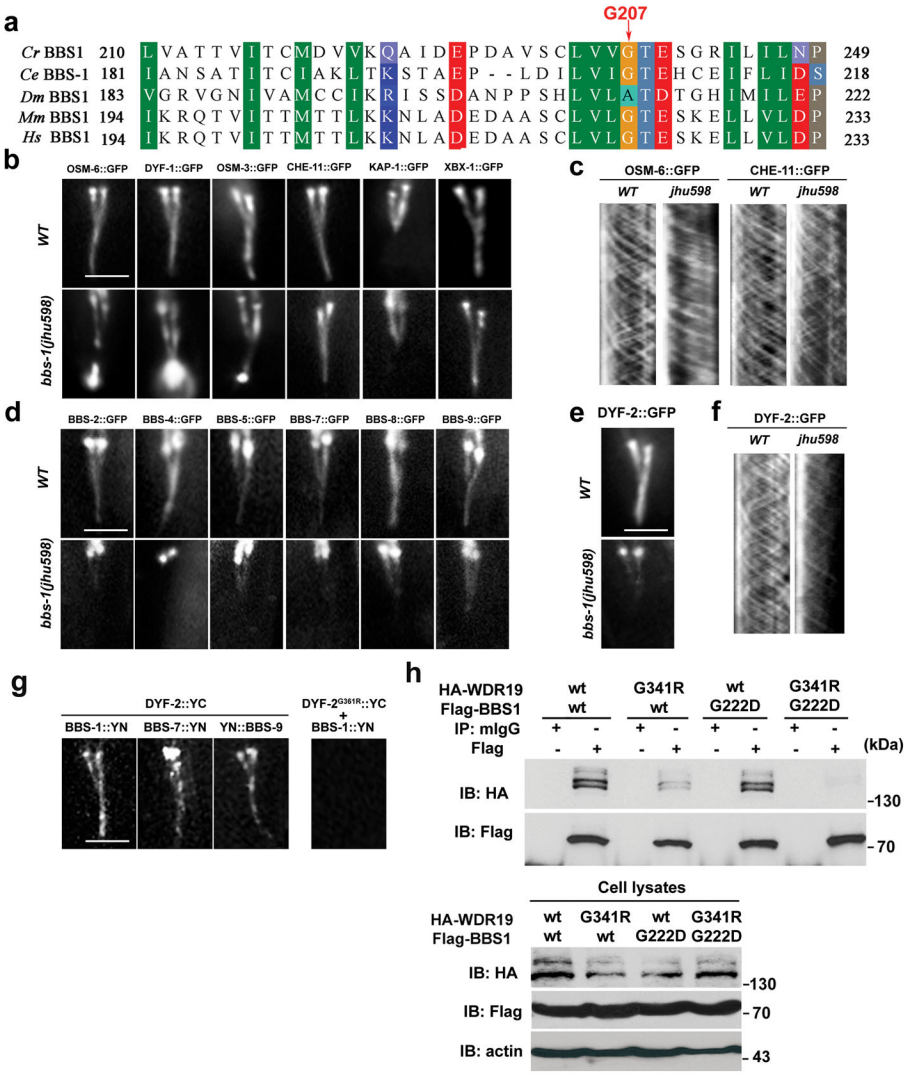

Figure 4. The BBSome and DYF-2 coordinate IFT assembly and turnaround at the ciliary tip

a, BBS-1 G207 site is conserved across species. *Cr, Chlamydomonas reinhardtii; Ce, Caenorhabditis elegans; Dm, Drosophila melanogaster; Mm, Mus musculus; Hs, Homo sapiens.* **b,** In *bbs-1(jhu598)*, IFT-B components (OSM-6, DYF-1) and IFT-B associated motor OSM-3, but not IFT-A component CHE-11 and IFT-A associated kinesin-II KAP-1and the retrograde dynein motor XBX-1, accumulate at the cilia tip. **c,** In *bbs-1(jhu598)* cilia, the IFT-B protein OSM-6::GFP shows normal anterograde but greatly reduced retrograde movement, whereas the IFT-A protein CHE-11 exhibits normal anterograde and retrograde movements. **d,** In *bbs-1(jhu598),* all BBSome subunits show absent or greatly reduced ciliary targeting. **e,** DYF-2 protein ciliary targeting is also greatly reduced in *bbs-1(jhu598)* cilia. **f,** Residual ciliary DYF-2 protein show active bidirectional IFT movement. **g,** In BiFC analyses, fluorescence complementation can be visualized between YC-tagged DYF-2 and either one of YN-tagged BBS-1, BBS-7, and BBS-9, but not between YC-tagged DYF-2^{G361R} and YN-tagged BBS-1. **h,** HEK293 cells were transiently transfected with HA-tagged WDR19 and Flag-tagged BBS1 constructs. 48 hours later, cells

were subjected to immunoprecipitation using normal mouse IgG (mIgG) or anti-Flag antibody. In all figures: bar, 5 μm.

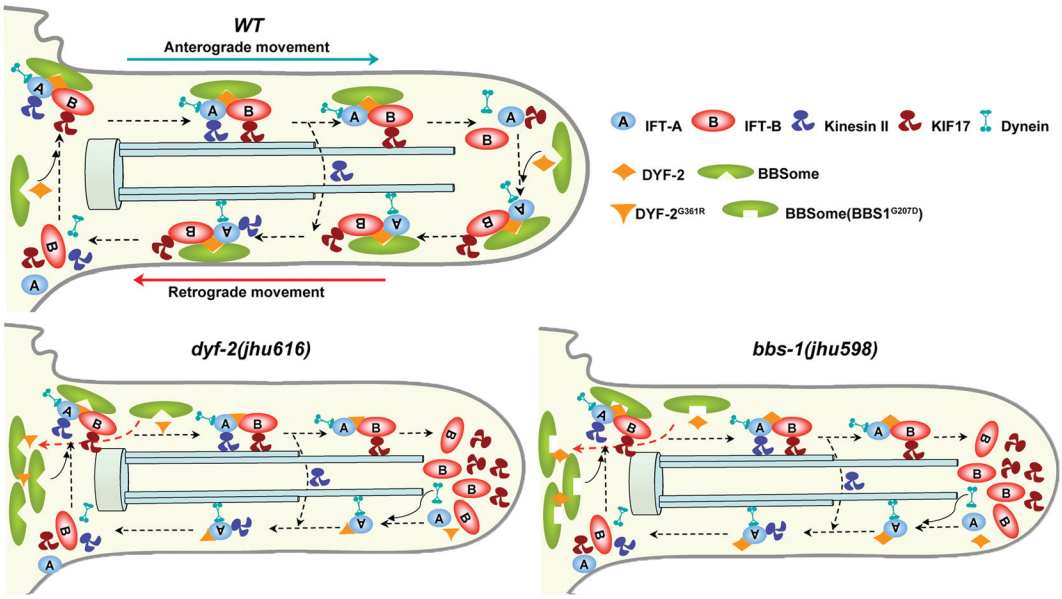

Figure 5. Model for the role of the BBSome in IFT assembly and turnaround

At the ciliary base in wild-type cells, the BBSome organizes IFT-A, IFT-B, and kinesin motors into a functional complex. DYF-2 stabilizes the association between the BBSome and IFT complex. This stabilization is mediated through the DYF-2 WD40 domain and BBS-1 and may also involve other BBS proteins. IFT particles dissociate after reaching the ciliary tip, and then the BBSome and DYF-2 coordinate to reorganize the entire IFT complex to ready it for retrograde transports. In *dyf-2(jhu616)* or *bbs-1(jhu598)* cilia, the BBSome is still functional at the ciliary base, as evident by the observation that IFT-A and IFT-B associate in anterograde transports, whereas the docking of the BBSome onto moving IFT particles is severely abrogated. The absence of the BBSome at the ciliary tip leads to defective reassembly of the IFT complex and the specific accumulation of IFT-B components at the ciliary tip. Note that although DYF-2^{G361R} or DYF-2 in *bbs-1(jhu598)* is put on moving IFT particles in this model, both of them show severely reduced ciliary targeting.